

RSC Advances



This is an *Accepted Manuscript*, which has been through the Royal Society of Chemistry peer review process and has been accepted for publication.

Accepted Manuscripts are published online shortly after acceptance, before technical editing, formatting and proof reading. Using this free service, authors can make their results available to the community, in citable form, before we publish the edited article. This *Accepted Manuscript* will be replaced by the edited, formatted and paginated article as soon as this is available.

You can find more information about *Accepted Manuscripts* in the [Information for Authors](#).

Please note that technical editing may introduce minor changes to the text and/or graphics, which may alter content. The journal's standard [Terms & Conditions](#) and the [Ethical guidelines](#) still apply. In no event shall the Royal Society of Chemistry be held responsible for any errors or omissions in this *Accepted Manuscript* or any consequences arising from the use of any information it contains.

ARTICLE

Synthesis and properties of a meso tris-ferrocene appended zinc(II) porphyrin and a critical evaluation of its dye sensitised solar cell (DSSC) performance

Cite this: DOI: 10.1039/x0xx00000x

Received 00th January 2012,
Accepted 00th January 2012

DOI: 10.1039/x0xx00000x

www.rsc.org/

D. Sirbu,^a C. Turta,^{b*} A. C. Benniston,^{b*} F. Abou-Chahine,^c H. Lemmetyinen,^c N. V. Tkachenko,^{c*} C. Wood^d and E. Gibson^{d*}

A zinc(II) porphyrin derivative, **F3P**, was prepared containing a single ferrocene group appended at three of the meso positions. The final meso position contains a benzoic acid unit, and was designed to be an anchoring moiety to a semiconductor surface. The cyclic voltammogram for the porphyrin derivative reveals that the three ferrocene units are oxidised and reduced at $E_{1/2} = +0.04$ V vs Fc^+/Fc . Other redox responses are porphyrin-based at +1.1 V vs Fc^+/Fc (irreversible) and -1.87 V and -2.20 V vs Fc^+/Fc (both quasi-reversible). The room temperature Mössbauer spectrum for **F3P** comprises of a doublet (δFe 0.44 mm/s; ΔEQ 2.35 mm/s; peak width 0.27 mm/s). The data are consistent with the ferrocene groups non-interacting with the porphyrin moiety in the ground state. Excitation of the compound in THF with an ultra-short laser pulse produces in less than 1 ps the charge separated state which comprises $\text{Fc}^+-\text{porp}^-$ and decays back to the ground state in 24 ps. Roughly the same behaviour is observed for the dye absorbed on TiO_2 , the only slight difference is the appearance of a long-lived component in the decay records. The electron for the porphyrin radical anion does not inject into the conduction band of the TiO_2 , only the porphyrin excited state participates in any electron injection process. Partly because of this factor the performance of the dye attached to TiO_2 in a DSSC device is rather limited ($J_{\text{SC}} = 0.068$ mA cm^{-2} , $\text{VOC} = 283$ mV, $\text{FF} = 0.42$, $\eta = 0.008\%$).

Introduction

Porphyrins and comparable derivatives are ubiquitous in Nature and constitute the molecular cornerstone of several light-driven processes which help maintain life on Earth.¹ The good cross-section capture of visible photons for the chromophores, coupled to their excellent redox excited-state behaviour are but two reasons for the continued interest in porphyrin derivatives.² Mimicry systems for artificial photosynthesis applications is certainly one major research area in which porphyrin derivatives have a special place.³ The manufacture of molecular dyads,⁴ triads and tetrads^{5,6} for propagating efficient, directional and long-lived charge separation continues to be of intense interest. Coupled to such fundamental studies is the application of porphyrin derivatives in areas such as sensors,⁷ PDT sensitisers⁸ and dye sensitised solar cells (DSSC).⁹ In regard to the latter case the direct conversion of sunlight to electricity is of major relevance because of its potential application to low-power technologies and the large-scale manufacture of

devices by simple wet chemistry processing.¹⁰ The basic working of DSSC relies on the injection of an excited state electron into the conduction band of an appropriate n-type semiconductor.¹¹ The classic material used is TiO_2 . The hole left behind on the sensitizer dye is plugged by a redox shuttle and the circuit is completed by the electron from the conduction band reducing via a secondary electrode the oxidised redox relay.¹² Numerous reports are available discussing the different processes in DSSC and trying to identify the "bottle-neck" which is limiting the efficiency of manufactured devices.¹³ There is one argument that charge must be shifted away from the semiconductor surface rapidly to generate long-lived charge-separated species.¹⁴ The analogy with natural photosynthetic reaction centre complexes is clear,¹⁵ but like in Nature the required assemblies to perform such task become more intricate. A challenge is to identify rudimentary molecular systems that may perform secondary charge shift.¹⁶ The most basic porphyrin-based molecular system is exemplified in Figure 1 incorporating meso ferrocene groups. The cartoon represents the basic working of the system

following excitation of the porphyrin moiety, where process 1 is oxidation of a ferrocene by the excited state and process 2 is charge recombination. It could be argued that if charge injection from the porphyrin excited state (process 3) competed with process 1 then the system would operate. Alternatively, if electron injection from the porphyrin anion (process 4) was fast and efficient then the energy wasting recombination process 2 would become less significant. We are, of course, not considering the recombination process involving back electron transfer from the conduction band of the TiO_2 . Evidently, knowledge of the intramolecular chromophore electron transfer events is critical. Prior work by Nadochenko and co-workers suggested for the free-base tetraferrocenyl porphyrin that processes 1 and 2 occurred in around 200 fs and 17 ps, respectively.¹⁷ There are no reports on the zinc(II) analogue. In this work we consider the zinc(II) tris-ferrocenylporphyrin **F3P** and elucidation of its properties especially probing the rates for processes 1 to 4. The dye attaches to TiO_2 but performance in a DSSC is limited.

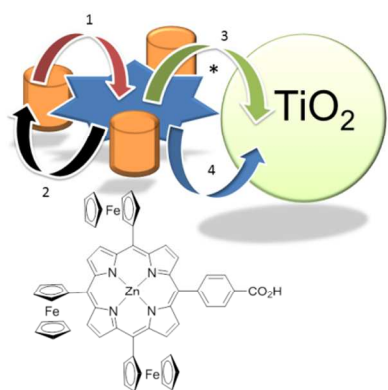


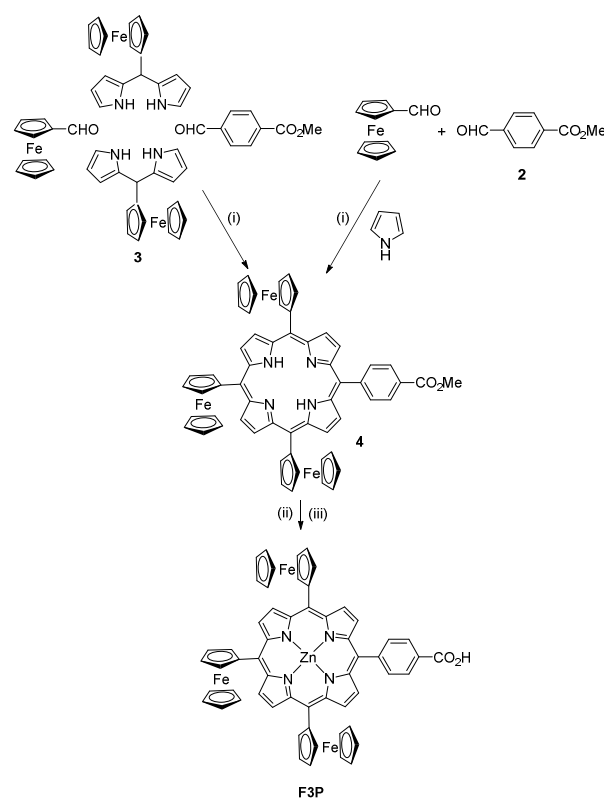
Figure 1. Top: Simple cartoon showing potential electron transfer pathways following excitation of the zinc(II) porphyrin. 1: charge separation involving oxidation of a ferrocene; 2: charge recombination; 3: electron injection into conduction band of TiO_2 from the zinc-porphyrin excited state; 4: electron injection into conduction band of TiO_2 from the porphyrin radical anion. Bottom: Tris-ferrocene zinc(II) porphyrin, **F3P**, containing the carboxylic acid anchoring unit.

Results and Discussion

Synthesis

Preparation of symmetrical porphyrin derivatives is relatively undemanding requiring only a suitable aldehyde to couple with pyrrole in the presence of acid.¹⁸ Complexity is introduced when the requirement is to have non-identical *meso* aryl groups, and have them proximal or distal to each other in the case of bis-aryl derivatives. Various methods to control the spatial location of aryl-*meso* groups were introduced by Lindsey and co-workers.¹⁹ Since we only required the presence of a single aryl carboxylate group, the simplest approach was to incorporate three ferrocene groups. Two strategies were attempted for the preparation of **F3P** via the free-base porphyrin and are illustrated in Scheme 1. Certainly the most uncomplicated method is the condensation of **2** with three equivalents of ferrocenecarboxaldehyde in the presence of pyrrole and trace acid. The drawback with this approach is the number of side-products formed by competing aldehyde-pyrrole coupling reactions (e.g., 2+2, 4+1). However, following very careful column

chromatography on silica gel, **4** was isolated in 14% yield as a purple solid. The alternative strategy involved the use of the preformed 5-ferrocenyldipyrromethane **3**²⁰ and its condensation with **2** and ferrocenecarboxaldehyde. Despite what may appear to be a better method the final yield was only slightly improved to 18%, probably because of the scrambling reactions. ¹H NMR spectra recorded for samples of **4** prepared by both methods were identical. The final two reactions of incorporation of zinc(II) into the porphyrin ring and ester hydrolysis worked in high yield to afford the desired compound **F3P**. Full characterisation of **F3P** by ¹H-, ¹³C- and DEPT-135° NMR spectra, as well as two-dimensional homo-(¹H/¹H COSY-45°) and heteronuclear (¹H/¹³C HSQC and HMBC) correlation spectra corroborated the structure. The FTIR spectrum for **F3P** displayed a strong stretch at 1690 cm^{-1} in agreement with presence of the carboxylic acid. The MALDI mass spectrum for **F3P** contained a cluster of peaks at $m/z = 1044$ and a theoretical pattern which agreed with the observed data. There was an additional peak at $m/z = 1061$ which can be assigned to a deprotonated water adduct.



Scheme 1. Reagents and Conditions: (i) DCM, TFA, DDQ, RT; (ii) $\text{Zn}(\text{OAc})_2 \cdot 2\text{H}_2\text{O}$, MeOH; (iii) NaOH, MeOH/ H_2O /THF, reflux.

Molecular Orbital Calculations

Previous work by Nemykin and co-workers²¹ determined the frontier molecular orbital picture for free-base tetra-ferrocene porphyrin derivatives. Part of this study was to rationalize the observation that as the number of ferrocene groups in *meso*(ferrocenyl) containing porphyrins increased there are subtle shifts in both the Q- and B-bands in their absorption spectra. Part of the reason is introduction of HOMOs associated with the ferrocene units into the overall MO picture, and potential charge transfer contributions to the absorption envelope. Considering these previous findings we felt it was prudent

to map out a clear MO picture for **F3P**. For a typical calculation the ground-state structure of **F3P** was modelled using a semi-empirical (AM1) method. The obtained structure was then refined further using DFT (B3LYP) and the 3-21G* and 6-31G(d) basis sets. Prior work by Slota *et al.*²² suggested that B3LYP with the LanL2DZ basis set is more conducive to collecting accurate structures for large metalloporphyrin molecules. The alternative employed by Nemykin *et al.*²³ was the Perdew nonlocal correlation function (B3PW91). Hence, calculations were re-run under more complex basis sets for comparison purposes (Table 1). There is a definite increase in the Zn-N bond lengths (*ca.* 2 % - 4 %) by changing the basis set from 3-21G* to 6-31G (d) to LanL2DZ and to B3PW91 6-31(d); values for the latter three methods are more consistent with crystallographically determined bond lengths (Zn-N 2.04 Å). It is very noticeable that the average Fe-C (ferrocene) bond lengths calculated using B3LYP (LanL2DZ) are longer than corresponding values returned from the other methods. The average crystallographically determined Fe-C bond length for ferrocene is 2.05 Å. The molecular picture for **F3P** is only slightly modified depending on the method and a representative structure is shown in Figure 2. Consistent with previous calculations is the observed “bowing” of the porphyrin ring. And the ferrocene units, because of unfavourable steric interactions, are twisted relative to the plane of the porphyrin ring. The barrier to rotation of the ferrocene group around the connector meso axis has been previously estimated to be in the order of 0.9 kcal mol⁻¹, and so in solution ferrocene internal rotation is very likely.²⁴

Table 1. Comparison of selected bond lengths calculated by DFT for **F3P**.^a

Method	Average Zn-N Bond Length / Å	Average Fe-C bond length / Å
B3LYP 3-21G*	1.98	2.05 (free); 2.04 (meso)
B3LYP 6-31G(d)	2.03	2.06 (free); 2.06 (meso)
B3LYP LanL2DZ	2.06	2.13 (free); 2.13 (meso)
B3PW91 6-31(d)	2.02	2.03 (free); 2.04 (meso)

^a Calculated using the programme Gaussian 03.

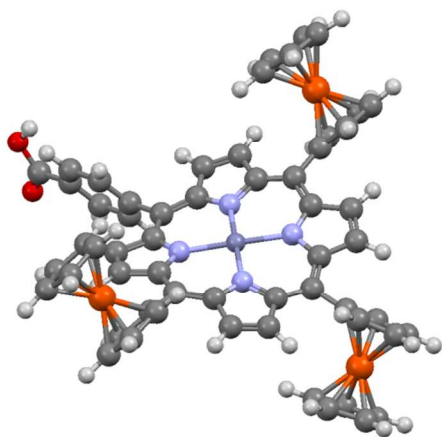


Figure 2. Energy-minimised computer calculated structure for **F3P** using DFT (B3PW91) and a 6-31G(d) basis set.

From the four calculations the two most consistent molecular orbital diagrams were obtained using B3PW91 6-31(d), B3LYP 6-31G(d)

and B3LYP LanL2DZ; in the latter the basis set core electron are frozen (48 for F3P). The frontier molecular orbital picture calculated by B3LYP 3-21G* was slightly different to the other two cases. We have taken the MO picture from the B3PW91 6-31(d) calculation (Figure 3) to be a more comprehensive picture, and collected in Supporting Information are MO pictures from the other three calculations. The HOMO is predominantly localised on the three ferrocene moieties, whereas the HOMO-1 is exclusively porphyrin based. The MOs HOMO-2 to HOMO-6 are entirely ferrocene centred. In turns out that the LUMO and LUMO+1 are degenerate and porphyrin-based π^* orbitals in agreement with Gouterman's four orbital model.²⁵ Both orbitals are well separated in energy from the LUMO+2 which resides on the meso benzoic acid group. Very crudely the HOMO-LUMO gap represents ferrocene-to-porphyrin charge transfer, the energy difference being 2.59 eV (479 nm).

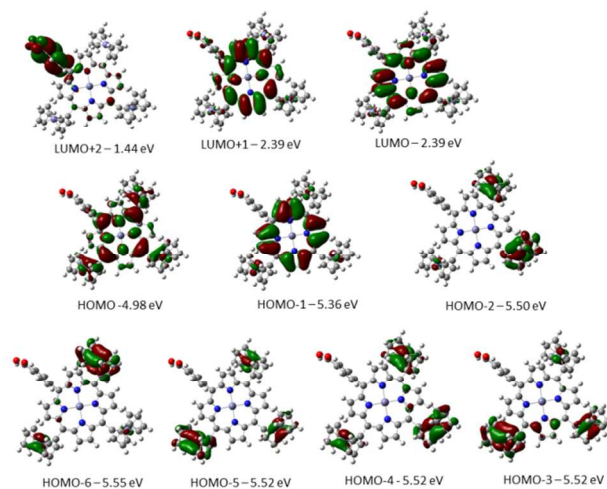


Figure 3. Selected molecular orbitals for **F3P** calculated by DFT (B3PW91) and using a 6-31G(d) basis set.

Electrochemistry and Absorption Spectroscopy

The redox behaviour for **F3P** was measured by cyclic voltammetry in dry THF using 0.2 M TBATFB as background electrolyte. DCM afforded rather poor results probably because of solubility problems. The cyclic voltammogram (Supporting Information) reveals redox processes associated with both the porphyrin and ferrocene groups. On the oxidation side of the CV a clear quasi-reversible wave is observed at +0.04 V vs Fc⁺/Fc, which is associated with redox at the ferrocene sites. No splitting of the wave is seen but the peak's separation difference of 180 mV would suggest that there are a series of overlapping waves. At a more positive potential an irreversible wave is observed at +1.1 V vs Fc⁺/Fc which is porphyrin-based oxidation. Upon scanning to negative potentials two quasi-reversible one-electron waves are seen at -1.87 V and -2.20 V vs Fc⁺/Fc and are again associated with redox at the porphyrin site. The overall redox behaviour for **F3P** is consistent with previous work carried out on ferrocenyl-porphyrin derivatives.^{21,26} It is worth noting that the computer calculated difference in energy between oxidation of a ferrocene (HOMO) and porphyrin (HOMO-1) is only 380 mV. The much larger value found electrochemically (*ca.* 1V) is rationalised, in part, by the large electrostatic repulsion created by a tri-positive charge so close to the porphyrin core.

The room temperature electronic absorption spectrum for **F3P** in chloroform is shown in Figure 4. The spectrum comprises a strong

Soret B-band at 431 nm ($1.6 \times 10^5 \text{ M}^{-1} \text{ cm}^{-1}$) typical of a divalent metalloporphyrin and a much weaker Q-band at 661 nm ($1.7 \times 10^4 \text{ M}^{-1} \text{ cm}^{-1}$). The weak band at 310 nm ($2.1 \times 10^4 \text{ M}^{-1} \text{ cm}^{-1}$) may be assigned to the lesser discussed porphyrin N-band. The Soret band also contains a shoulder in the region of ~ 490 nm which is ascribed by Nemykin *et al.* to predominantly ferrocene-to-porphyrin charge transfer. Certainly this interpretation is consistent with the computer calculated energy-gap discussed previously. The absorption in the visible spectrum of the porphyrin is improved in the region between Soret and Q bands compared to the tetra-phenyl porphyrin analogue.²⁷

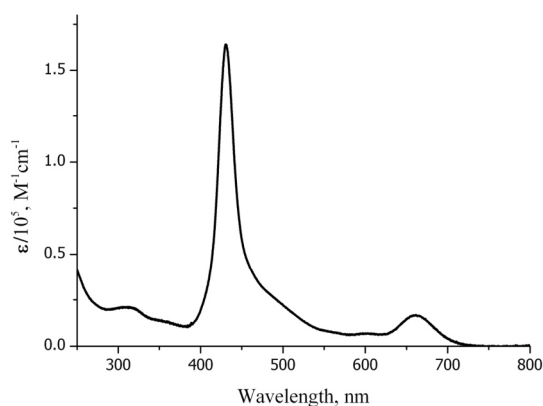


Figure 4. Room temperature UV-Vis absorption spectrum for **F3P** in chloroform.

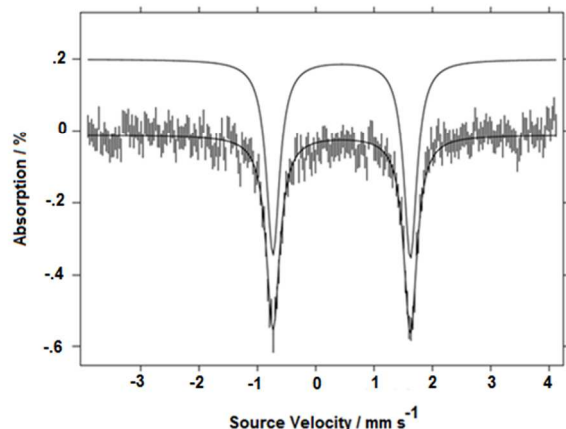


Figure 5. Room temperature ^{57}Fe -Mössbauer spectrum for **F3P** showing the characteristic doublet pattern.

^{57}Fe Mössbauer Spectroscopy

The room temperature Mössbauer spectrum for **F3P** is shown in Figure 5 with pertinent parameters presented in Table 2. Also included are data for the reference compound zinc(II) tetraferrocenylporphyrin (**ZnTFP**).²⁸ The isomer shift δ and large quadrupole splitting ΔE_Q for the clear doublet are typical for low-spin iron (d^6) ferrocene derivatives. The comparison of **F3P** and unsubstituted ferrocene²⁹ data shows that the porphyrin core has no major influence on the electron density at the iron nucleus, despite the close proximity of the ferrocene and porphyrin groups. The presence of only one doublet and the narrow line width, Γ , indicates

that the three ferrocene moieties are essentially identical. It is worth noting that no ferrocenium assignable signals are observed, which would be present if partial oxidation had occurred. At least in the ground state and solid state the compound **F3P** behaves as if it comprises isolated ferrocene and porphyrin subunits.

Table 2. Experimental Mössbauer parameters for **F3P** and reference compounds at room temperature.

Compound	δ , mm/s	ΔE_Q , mm/s	Γ , mm/s
ZnTFP ^a	0.45	2.55	na
F3P	0.44	2.35	0.27
Fc ^b	0.44	2.35	na

^{a,b}Reference compounds as discussed in the text taken from references 28 and 29.

Dye Sensitised Solar Cell Performance

Since the I^-/I_3^- electrolyte couple does not have enough driving force to reduce the ferrocene, photovoltaic experiments were conducted in a cell using $\text{Co}(\text{II})$ tris(4,4'-di-methoxy-bipyridine) perchlorate ($E^0 = -0.26 \text{ V}$ vs. Fc^+/Fc). The electrolyte consisted of 0.1 M $\text{Co}(\text{II})$ tris(4,4'-di-methoxy-bipyridine) perchlorate, 0.1 M 4-tert-butylpyridine, 0.2 M, tert-butyl ammonium perchlorate and 0.015 M NOPF₆ in propylene carbonate as solvent. The plot of photocurrent density versus voltage (under standard AM 1.5 global sunlight at 1000 W/m^2 and a temperature of 298 K) for **F3P** is shown in Figure 6. The experiment was repeated in darkness and proved the photovoltaic nature of the effect. The short circuit current density was found to be 0.068 mA cm^{-2} , the open circuit voltage was 283 mV, the fill factor was 0.42 and the power conversion efficiency (η) was evaluated to be 0.0081%. Each of these values are extremely low and **F3P** can be considered a poor sensitizer for a DSSC.

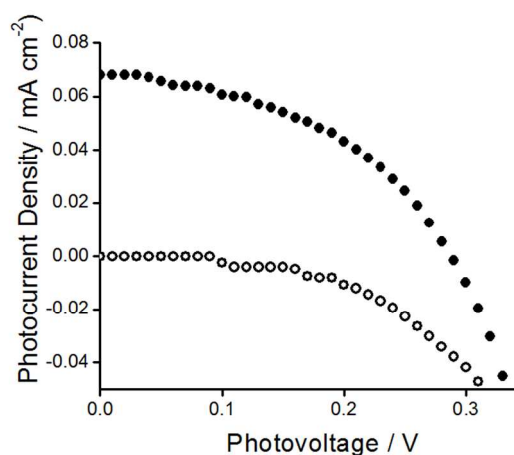


Figure 6. Example of an I-V curve (\circ = dark, \bullet = light) for a **F3P** based dye sensitized solar cell using $\text{Co}(\text{II})$ (4,4'-dimethoxy-2,2'-bipyridine)₃(ClO₄)₂ 0.1 M, 4-tert-butylpyridine 0.2 M, tert-butyl ammonium perchlorate 0.1 M and NOPF₆ 0.015 M in propylene carbonate. $V_{OC} = 0.28 \text{ V}$ and $J_{SC} = 0.068 \text{ mA cm}^{-2}$.

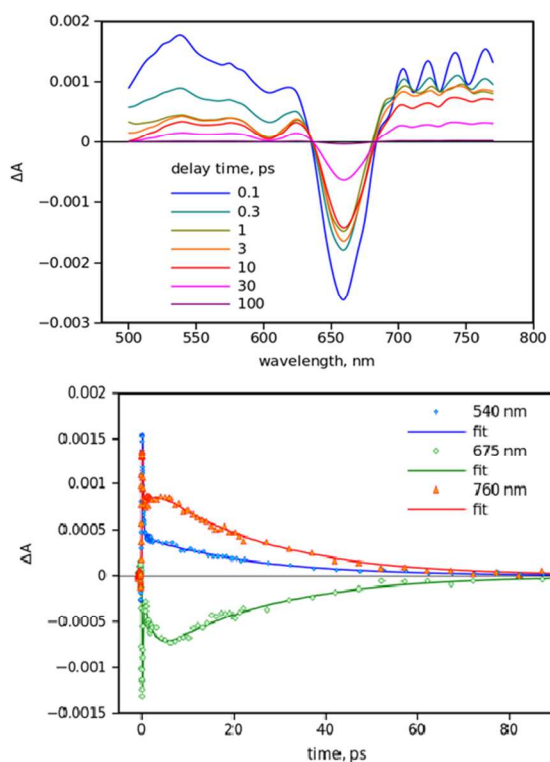


Figure 6. Selected transient absorption spectra recorded after excitation of **F3P** in THF with a 70 fs laser pulse delivered at 480 nm (top). Transient absorption decay profiles of **F3P** in THF at selected wavelengths (bottom). Symbols are measured data and lines are fit curves.

Pump-Probe Spectroscopy

The excited-state property for **F3P** was elucidated using femtosecond pump-probe spectroscopy in MeCN and THF. The latter solvent was found to be much better and avoided unnecessary precipitation of the material during data collection. The compound was excited with a 70 fs laser pulse at 480 nm which almost exclusively populates the S_2 (Soret) state of the porphyrin. Time resolved transient absorption spectra with compensated group velocity dispersion are presented in Figure 6, along with decay profiles at a few selected wavelengths. The measurements were also fitted globally to three and four exponential models. Although a four exponential fit gave roughly a 15% improvement of the sigma value it mainly resulted in a very short-lived component (80 fs) which arises most probably from “non-exponential” fast thermal relaxation and will not be discussed further.

There is an almost instantaneous bleach in the region around 660 nm corresponding to the Q-bands of the porphyrin. To the low energy side of this bleach is a broad profile which is assigned to the zinc-porphyrin radical anion.³⁰ It is not possible to identify the ferrocenium ion because of its low molar absorption coefficient, but it must be produced as part of the charge transfer process to account for the anion. The results from a global fit of the spectroscopic data are presented in Figure 7, and shows the decay component spectra (curves with symbols) and time-resolved transient spectra right after the excitation (at 0 ps) and after fast relaxation with 0.19 ps time constant (at 1 ps). An interesting feature is that initial bleaching of the Q-band at 670 nm recovers by roughly half with a time constant

of 0.19 ps, but then the bleaching increases by one third with a time constant 2.5 ps before complete recovery with a time constant of 24 ps. The interpretation of the results is not straightforward, though it is noticeable that the 2.5 ps component does not affect the spectrum much outside the Q-band region. Tentatively this component can be attributed to conformation changes associated with the charge separated (CS) state. The fast time constant is presumably formation of the CS state. The S_2 to S_1 conversion in zinc tetraphenylporphine is, depending on the solvent, on the order of 1-3.5 ps. There are reports of energy and electron transfer from the S_2 state of zinc porphyrin adducts.³¹ Considering the rate for charge separation we cannot discount that the process is competing with internal conversion. The charge recombination process though slower by comparison is still extremely rapid and reforms the ground state in $\tau = 24$ ps. This measured value is very similar to that reported by Nadtochenko and co-workers for a free-base porphyrin analogue.¹⁷ The presence of the zinc(II) ion appears to have no real affect on the charge recombination process.

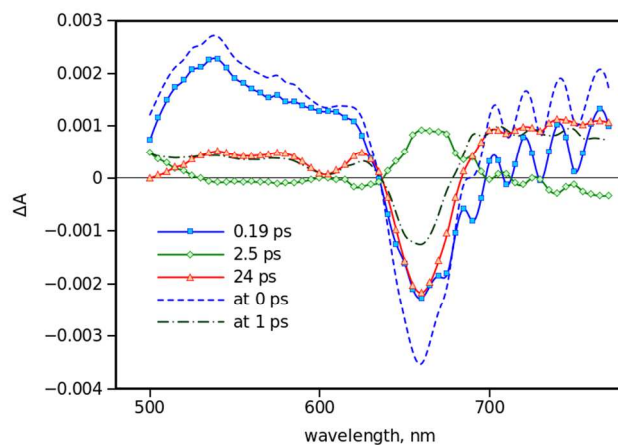


Figure 7. Decay component spectra (lines with symbols) and time-resolved spectra at 0 and 1 ps delay time for **F3P** in THF.

The behaviour for **F3P** attached to TiO_2 was also measured and compared to a control compound containing phenyl groups instead of the ferrocene moieties (**ZnTPP**). Time-resolved transient absorption spectra are presented in Supporting Information, and except for a relatively weak long-lived component the results are similar to those obtained in THF solution. The rather good agreement between the transient absorption responses for **F3P** in solution and attached to TiO_2 indicates that charge separation (CS) in the molecule is not affected by the presence of TiO_2 surface. Another significant finding is electron injection from the porphyrin anion to the TiO_2 does not take place in the lifetime of the CS state (29 ps). It is very noticeable (Figure 8) that the minor long-lived component has clear bleaching of the porphyrin Q-band and probably comes from direct injection of electron from the photo-excited porphyrin into the TiO_2 . This is the only indication of possible electron injection and its low intensity is in good agreement with the low efficiency of the DSSC.

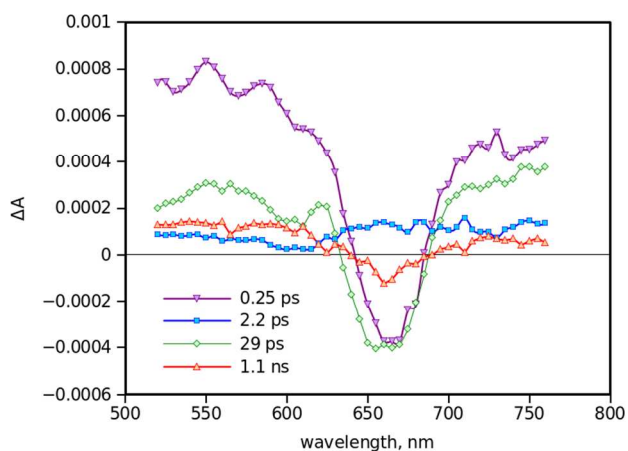


Figure 8. Decay component spectra obtained from global fit of transient absorption data for **F3P** on TiO_2 .

The decay component spectra for **ZnTPP** attached to TiO_2 are very different to those shown in Figure 8 (see Supporting Information). The fast component, 0.13 ps, can be attributed to electron injection into the TiO_2 because of the broad negative band around 670 nm, which is assigned to the porphyrin cation. Further re-shaping of the cation band takes place with a time constant of 3.1 ps and is in qualitative agreement with other similar systems. Recombination is also a “multi-exponential” process with lifetimes in the range from few tens of picoseconds to nanoseconds.

Evaluation of Excited State Deactivation for DSSC Application

The excited state spectroscopic data for **F3P** attached to TiO_2 shows unequivocally that the dye is rather poor at injecting electrons into the conduction band of the semiconductor TiO_2 . Generally electron injection into TiO_2 is extremely fast and in the order of 300 fs.³² For the control compound the excited state porphyrin injects electrons in around 130 fs. Assuming this latter value is the same for **F3P** the maximum yield of electrons into the TiO_2 conduction band is only 60%. It is clear that injection of an electron from the photo-generated porphyrin anion (Figure 1) into the TiO_2 conduction does not take place. One possible reason for this is the rather strong coupling between the electron and hole due to the short distance between the donor and acceptor.³³ This interpretation would mean that the CS state is not a “real” radical ion pair, but rather an electron density redistribution. It is noted that the driving force is very favourable for anion injection and estimated from electrochemistry data ($E_{\text{red}} = -1.5$ V vs NHE) and the conduction band energy for TiO_2 (-0.5 V vs NHE) to be around 1.0 eV. There is the possibility that the reduction potential for the porphyrin is altered by its attachment to the TiO_2 and the driving force is much smaller.

Considering that direct electron injection from the porphyrin excited state (process 3 Figure 1) occurs, it is very probable that hole transfer to the appended ferrocene (process 1 Figure 1) also takes place to generate the ferrocenium ion. Given that the $\text{Co}^{2+}/\text{Co}^{3+}$ couple for the cobalt bipyridyl- and terpyridyl- based electrolytes have redox potentials of -0.21 V and -0.32 V vs Fc^+/Fc ,³⁴ then again it is feasible that the redox shuttle process should proceed in a DSSC incorporating **F3P**. Other contributing factors to the very low photocurrent are twofold. One evident problem is the close proximity of the ferrocene groups to the semi-conductor surface which will facilitate charge recombination. Even the presence of a blocking layer on the TiO_2 surface may not be sufficient to prevent back electron transfer. There is the additional argument that

ferrocenium/ ferrocene may not be conducive for coupling to the cobalt(II/III) electrolyte redox relay because of slow electron exchange kinetics.³⁵

Conclusions

In the preparation of the trisubstituted ferrocene-based porphyrin derivative it would appear that the “one-pot” stoichiometry-correct reaction works as well as the preorganised method starting from a ferrocene-dipyrromethane precursor. The only advantage of the second method is the slightly easier purification of the final product. The final zinc(II) compound is an analogue of meso-ferrocenyl porphyrins recently prepared by Rochford *et al.*³⁶ for evaluation as sensitizers in DSSC. Although the group published no measurements our studies would suggest that performance will be poor especially for derivatives where ferrocenes are close to the anchoring carboxylic acid group. However, it will be interesting to see if an improved response is observed for compounds where the ferrocene is trans to the carboxylic acid anchoring unit. The ferrocenium produced would be away from the semiconductor surface and we could expect charge recombination to be much slower. Despite this our results clearly show that only direct photo-injection from the porphyrin excited state is relevant for the outlined ferrocene-porphyrin derivatives. Hence in the design of porphyrin-based systems for DSSC applications strongly coupled donor-acceptor pairs should be avoided.

Experimental

^1H -, ^{13}C - and DEPT-135° NMR spectra, as well as two-dimensional homo- ($^1\text{H}/^1\text{H}$ COSY-45°) and heteronuclear ($^1\text{H}/^{13}\text{C}$ HSQC and HMBC) correlation spectra were recorded with Bruker – Avance-III 400 MHz and Jeol ECS-400 MHz. Chemical shifts for ^1H - and ^{13}C -NMR spectra are referenced relative to TMS or the residual protiated solvent. IR spectra were recorded with Perkin Elmer Spectrum 100 FT-IR Spectrometer. Elemental analysis was performed on Elemental Vario EL3 machine. Atomic absorption spectra were measured using AAS-3 machine. Electronic absorption spectra were recorded using a Hitachi U3310 spectrophotometer. The ^{57}Fe -Mössbauer spectrum was acquired at room temperature (RT) using a conventional spectrometer in the constant-acceleration mode (MS4, Edina, USA) equipped with a ^{57}Co source (3.7 GBq) in a rhodium matrix. Isomer shifts are given relative to $\alpha\text{-Fe}$ at RT. The spectrum was fitted using the Mössbauer fitting program (Edina).

Cyclic voltammetry experiments were performed using a fully automated HCH Instruments Electrochemical Analyzer and a three electrode set-up consisting of a glassy carbon working electrode, a platinum wire counter electrode and an Ag/AgCl reference electrode. Ferrocene was used as an internal standard. All studies were performed in deoxygenated DCM or THF containing TBATFB (0.2 M) as background electrolyte. Redox potentials were reproducible to within ± 15 mV.

Femto- to pico-second time-resolved absorption spectra were collected using a pump-probe apparatus consisting of a Libra F-1K (Coherent Inc.) generator producing 100 fs pulses with 1 mJ energy at 800 nm with a repetition rate of 1 kHz, and a Topas-C (Light Conversion Ltd.) OPA providing pump pulses in a wide spectrum range (UV-visible-near IR). The measurements part for the pump-probe method was a ExciPro (CDP Inc., Russia) equipped with two array detectors coupled to a spectrometer (CDP2022i) for probe

detection in the visible (300-1000 nm) and near IR (900-1700 nm) ranges. A white light continuum was used as the probe and was generated in a sapphire plate, and the overall time resolution of the instrument was 100-200 fs depending on the sample type and wavelength range.

Time-resolved transient absorption data were manipulated using the freely available software package, Decfit. In a typical analysis the whole collection of differential absorption spectra was inspected over the full timescale, and decay kinetics were obtained in the whole measured wavelength range with 5 nm step by averaging spectra in 5 nm intervals at each delay time. Lifetimes were obtained by global fit of the whole data set. Best fits were judged by the usual methods of remaining residuals and sigma value. Current-voltage (IV) characteristics were measured under 1000 Wm⁻² and 100 Wm⁻² AM 1.5 G illumination using a Newport solar simulator (model 91160) and a Keithley 2400 source/meter.

Solar Cell Preparation.

Fluorine-doped tin oxide (FTO) glass substrates (Pilkington, TEC15, sheet resistance 15 Ω/square) were cleaned in an ultrasonic bath overnight using (in order) ethanol, water and ethanol. The conducting glass substrates were pretreated by immersion in a 40 mM aqueous TiCl₄ solution at 70 °C for 25 minutes and then washed with water. Mesoporous TiO₂ films were prepared with an area of 0.25 cm² by screen printing two layers of transparent colloidal TiO₂ paste (Solaronix, **Ti-Nanoxide T/SP**) followed by one layer of a light-scattering TiO₂ paste (Solaronix, **Ti-Nanoxide R/SP**) and heated at 450 °C in an air atmosphere in an oven (Nabertherm LE 14/11/B150) for 30 minutes between deposition steps. The conducting glass substrates were post-treated by immersion in a 40 mM aqueous TiCl₄ solution at 70 °C for 25 minutes and then washed with water. The electrodes were gradually heated in an oven (Nabertherm LE 14/11/B150) at 450 °C in an air atmosphere.

TiO₂ films were immersed in a dye bath containing 0.28 mM **F3P** and 0.60 mM chenodeoxycholic acid in DCM and left at RT for 18 h. The films were then rinsed in ethanol to remove excess dye and dried at RT. Solar cells were assembled with a thermally platinized counter electrode (Pilkington TEC8, sheet resistance 8 Ω/square) using a 30 μm thick thermoplastic frame (Dyesol, Surlyn 1702). The electrolyte solution, containing either 1-propyl-3-methylimidazolium iodide 0.8 M, tert-butyl pyridine 0.3 M, iodine 0.1 M, and guanidinium thiocyanate 0.05 M in methoxypropionitrile (data not shown), or Co(4,4-dimethoxy-2,2'-bipyridine)₃ (ClO₄)₂ 0.1 M, 4-tert-butyl pyridine 0.2 M, tert-butyl ammonium perchlorate 0.1 M, NOPF₆ 0.015 M, in propylene carbonate, was introduced through the pre-drilled hole in the counter electrode, which was sealed afterwards with Surlyn and a glass cover slide.

Computer Calculations

Computational calculations were performed using a 32-bit version of Gaussian03³⁷ on a quadruple-core Intel Xeon system with 4GB RAM. The calculations were run in parallel, fully utilising the multi-core processor. Energy minimisation calculations were monitored using Molden and run in parallel with frequency calculations to ensure optimised geometries represented local minima.

Synthesis

All chemicals were purchased from commercial sources and used as received unless otherwise stated. Basic solvents for synthesis were dried using literature methods. Solvents for spectroscopic investigations were of the highest purity available.

Preparation of methyl 4-formylbenzoate dimethyl acetal (1)

Concentrated H₂SO₄ (3.2 mL, 60 mmol, 1.5 eq) was slowly added to a solution of 4-formylbenzoic acid (6 g, 40 mmol) in MeOH/CHCl₃ (130 mL/30 mL), and the resulting mixture was refluxed for 4 h. During the reaction water was removed by azeotropic distillation. The resulting reaction mixture was left to cooling to room temperature, poured into water (100 mL) and extracted with CHCl₃ (100 mL). The separated organic layer was washed with aqueous NaHCO₃ (10%, 2 x 50 mL) and distilled water (2 x 50 mL). The separated organic layer was dried over anhydrous Na₂SO₄, filtered and the solvent removed *in vacuo* to give **1** (6 g, 29 mmol, 71% yield). ¹H-NMR (400 MHz, CDCl₃, TMS, δ): 8.04 (d, *J* = 8.2 Hz, 2H, *o*-Ph), 7.53 (d, *J* = 8.2 Hz, 2H, *m*-Ph), 5.44 (s, 1H, formyl), 3.91 (s, 3 H, methyl ester), 3.32 (s, 6H, dimethyl acetal).

Preparation of Methyl 4-formylbenzoate (2)

A mixture of **1** (6 g, 28.6 mmol) and *p*-toluenesulfonic acid monohydrate (5.4 g, 28.4 mmol, 1 eq) in acetone (150 mL) was stirred at RT. When TLC analysis indicated that all the starting material was consumed (ca. 20 h) the reaction mixture was poured into CHCl₃ (200 mL). The solution washed with aqueous NaOH (10 %, 3 x 100 mL) and distilled water (100 mL). The organic layer was separated, dried over anhydrous Na₂SO₄, filtered and the solvent removed *in vacuo* to give **2** (4.6 g, 28.0 mmol, 98%). ¹H-NMR (400 MHz, CDCl₃, TMS, δ): 10.10 (s, 1H, formyl), 8.20 (d, *J* = 8.1 Hz, 2H, *o*-Ph), 7.95 (d, *J* = 8.1 Hz, 2H, *m*-Ph), 3.96 (s, 3H, methyl ester).

Preparation of 5-Ferrocenyldipyrromethane (3)

A solution of ferrocenecarboxaldehyde (4 g, 18.7 mmol) dissolved in pyrrole (50 mL, 0.75 mol, 40 eq) was bubbled with Ar for 15 mins. TFA (0.14 mL, 1.82 mmol, 0.1 eq) was added and the solution was stirred at RT in an Ar atmosphere. After 15 mins aqueous NaOH (0.1 M, 23 mL) was added to stop the reaction. The mixture was poured into water (40 mL) and extracted with ethyl acetate (60 mL). The collected organic layer was washed with distilled water (2 x 60 mL), separated and dried over anhydrous Na₂SO₄, filtered and solvent removed *in vacuo*. The obtained crude product was purified by chromatography on silica-gel using a petroleum ether (40 – 60 °C) : ethyl acetate (9:1) mixture as eluent, collecting the first brown coloured band. The solvent was removed *in vacuo* to give **3** (4.9 g, 14.8 mmol, 79%). ¹H-NMR (400 MHz, CDCl₃, TMS, δ): 7.87 (br s, 2H, NH), 6.64 (ddd, *J* = 2.6, 2.6, 1.6 Hz, 2H, H²+H^{2'}-pyrrole), 6.16 (dd, *J* = 5.9, 2.7 Hz, 2H, H³+H^{3'}-pyrrole), 6.02 (tdd, *J* = 2.3, 1.6, 0.7 Hz, 2H, H⁴+H^{4'}-pyrrole), 5.20 (s, 1H, methane), 4.16 (ap t, 2H, α-Cp), 4.09 (s, 5H, CpH), 4.08 (ap t, 2H, β-Cp). ¹³C NMR (101 MHz, CDCl₃, δ): 133.29 (C³+C^{5'}-pyrrole), 116.94 (C²+C^{2'}-pyrrole), 108.12 (C³+C^{3'}-pyrrole), 106.67 (C⁴+C^{4'}-pyrrole), 90.33 (C_pipso), 69.03 (CpH), 68.16 (β-Cp), 67.69 (α-Cp), 38.26 (methane).

Preparation of 5,10,15-Trisferrocenyl-20-(methyl 4-benzoate) porphyrin (4)

a) Synthesis from 5-Ferrocenyldipyrromethane

A mixture of **2** (0.25 g, 1.5 mmol), ferrocenecarboxaldehyde (0.32 g, 1.5 mmol, 1 eq), **3** (1.0 g, 3.0 mmol, 2 eq) and TFA (0.09 mL, 1.2 mmol, 0.8 eq) in CH₂Cl₂ (320 mL) was stirred at RT under an Ar atmosphere. When TLC analysis indicated that all ferrocenecarboxaldehyde was consumed (~ 2 h), DDQ (0.34 g, 1.5 mmol, 1 eq) was added and the mixture was refluxed for another 1.5 h. After this period the reaction mixture was deposited on silica-gel and chromatographed using CH₂Cl₂: MeOH (100 : 3) mixture as

eluent. The obtained crude product was purified by column chromatography on silica-gel using toluene : petroleum ether (40 – 60 °C) : (Et)₃N (15 : 10 : 1) mixture as eluent. The major green-brown fraction was collected, solvent reduced *in vacuo* and precipitate recrystallized from toluene/hexane mixture to give **4** (0.27 g, 0.27 mmol 18%) as a purple microcrystalline powder.

b) *Direct condensation of aldehydes*

A mixture of **2** (0.49 g, 3 mmol), ferrocenecarboxaldehyde (2.12 g, 9.9 mmol, 3.3 eq), pyrrole (1 mL, 14.4 mmol, 4.8 eq) and TFA (0.2 mL, 2.6 mmol, 0.87 eq) in CH₂Cl₂ (250 mL) was stirred at RT in Ar atmosphere. When TLC analysis indicated that all ferrocenecarboxaldehyde was consumed (1.5 h) DDQ (0.68 g, 3.0 mmol, 1 eq) was added and the mixture refluxed for another 1.5 h. After this period the reaction mixture was deposited on silica-gel and chromatographed using CH₂Cl₂ : MeOH : (Et)₃N (100 : 4 : 1) mixture as eluent. The obtained crude product was purified by two consecutive column chromatography on silica-gel using toluene : (Et)₃N (50 : 1) and toluene : petroleum ether (40 – 60 °C) : (Et)₃N (15 : 10 : 1) mixtures as eluent. The major green-brown fraction was collected, solvent reduced *in vacuo* and precipitate recrystallized from toluene/hexane mixture to give **4** (0.41 g, 0.41 mmol, 14% with respect to **2**) as a purple microcrystalline powder. ¹H-NMR (400 MHz, CDCl₃, TMS, δ): 9.76 (ap q, *J* = 4.8 Hz, 4H, β-pyrrole-Fc-Fc), 9.66 (d, *J* = 4.8 Hz, 2H, β-pyrrole-Ph-Fc), 8.53 (d, *J* = 4.8 Hz, 2H, β-pyrrole-Ph-Fc), 8.43 (d, *J* = 8.1 Hz, 2H, *m*-Ph), 8.23 (d, *J* = 8.1 Hz, 2H, *o*-Ph), 5.40 (ap t, *J* = 1.7 Hz, 6H, α-Cp_{1,3}), 4.80 (ap t, *J* = 1.7 Hz, 2H, β-Cp₂), 4.77 (ap t, *J* = 1.7 Hz, 4H, β-Cp_{1,3}), 4.12 (s, 3H, methyl ester), 4.02 (s, 15H, CpH_{1,2,3}), -1.12 (s, 2H, NH). ¹³C NMR (101 MHz, CDCl₃, δ): 167.51 (C-carboxylic), 147.15 (*i*-Ph), 146.0 – 147.0 (α-pyrrole-Ph-Fc, vbr), 145 – 147 (α-pyrrole-Fc-Fc, vbr), 143.5 – 144.5 (α-pyrrole-Ph-Fc, vbr), 134.48 (*o*-Ph), 131.47 (β-pyrrole-Ph-Fc), 131.18 (β-pyrrole-Fc-Fc), 130.55 (β-pyrrole-Fc-Fc), 129.76 (β-pyrrole-Ph-Fc), 129.57 (*p*-Ph), 128.15 (*m*-Ph), 118.53 (meso-C-Fc₂), 118.23 (meso-C-Ph), 118.00 (meso-C-Fc_{1,3}), 89.80 (C_i-Cp₂), 89.16 (C_i-Cp_{1,3}), 77.60 (α-Cp₂), 77.11 (α-Cp_{1,3}), 70.60 (CpH), 69.29 (β-Cp_{1,3}), 69.22 (β-Cp₂), 52.54 (C-methyl ester).

Preparation of Zn(II) 5,10,15-trisferrocenyl-20-(methyl 4-benzoate) porphyrin (5)

A solution of Zn(OAc)₂·2H₂O (220 mg, 1.0 mmol, 10 eq) in MeOH (8 mL) was added to a solution of free base **4** (100 mg, 0.1 mmol) in benzene (50 mL) with stirring at RT. When TLC analysis indicated that all starting material was consumed (2 h) the reaction mixture was washed with distilled water (3x50 mL), the solution dried over anhydrous Na₂SO₄, filtered and solvent removed *in vacuo* to give **5** (90 mg, 85 μmol, 85%) as a purple microcrystalline powder. ¹H-NMR (400 MHz, CDCl₃, TMS, δ): 10.01 (ap q, *J* = 4.8 Hz, 4H, β-pyrrole-Fc-Fc), 9.92 (d, *J* = 4.7 Hz, 2H, β-pyrrole-Ph-Fc), 8.65 (d, *J* = 4.7 Hz, 2H, β-pyrrole-Ph-Fc), 8.41 (d, *J* = 8.4 Hz, 2H, *m*-Ph), 8.24 (d, *J* = 8.4 Hz, 2H, *o*-Ph), 5.45 (ap t, *J* = 1.8 Hz, 2H, α-Cp₂), 5.43 (ap t, *J* = 1.9 Hz, 4H, α-Cp_{1,3}), 4.81 (ap t, *J* = 1.8 Hz, 2H, β-Cp₂), 4.78 (ap t, *J* = 1.8 Hz, 4H, β-Cp_{1,3}), 4.10 (s, 3H, methyl ester), 4.091 (s, 10H, CpH_{1,3}), 4.090 (s, 5H, CpH₂). ¹³C NMR (101 MHz, CDCl₃, δ): 167.58 (C-carboxylic), 150.68 (α-pyrrole-Ph-Fc), 150.13 (α-pyrrole-Fc-Fc), 149.76 (α-pyrrole-Fc-Fc), 148.31 (α-pyrrole-Ph-Fc), 147.98 (*i*-Ph), 134.45 (*o*-Ph), 132.70 (β-pyrrole-Ph-Fc), 131.92 (β-pyrrole-Fc-Fc), 131.77 (β-pyrrole-Fc-Fc), 130.34 (β-pyrrole-Ph-Fc), 129.44 (*p*-Ph), 128.01 (*m*-Ph), 119.46 (meso-C-Fc₂), 119.28 (meso-C-Ph), 118.81 (meso-C-Fc_{1,3}), 90.70 (C_i-Cp₂), 90.51 (C_i-Cp_{1,3}), 77.72 (α-Cp₂), 77.36 (α-Cp_{1,3}), 70.65 (CpH), 68.90 (β-Cp_{1,2,3}), 52.47 (C-methyl ester). Elemental analysis calcd for C₅₈H₄₂Fe₃N₄O₂Zn: C 65.72, H 3.99, N 5.29, found: C 66.60, H 4.25, N 5.15.

Preparation of Zn(II) 5,10,15-trisferrocenyl-20-(4-carboxyphenyl) porphyrin (F3P)

NaOH (53 mg, 1.33 mmol, 20 eq) in MeOH (8 mL) and H₂O (2 mL) was added to a solution of ester **5** (70 mg, 66 μmol) in THF (8 mL). The mixture was refluxed for 12 h under Ar atmosphere, then left for cooling over night at RT. CHCl₃ (70 mL) and water (70 mL) were added and mixture acidulated to pH = 6 with 2.0 M HCl. The resulting green/brown colored organic layer was separated, washed with water (3 x 50 mL), dried over anhydrous Na₂SO₄, filtered, solvent removed *in vacuo* and precipitate recrystallized from toluene/hexane mixture to give **6** (51 mg, 49 μmol, 74%) as a purple microcrystalline powder. ¹H-NMR (400 MHz, DMSO-d₆, δ): 9.86 (ap t, *J* = 5.3 Hz, 4H, β-pyrrole-Fc-Fc), 9.77 (d, *J* = 4.7 Hz, 2H, β-pyrrole-Ph-Fc), 8.52 (d, *J* = 4.7 Hz, 2H, β-pyrrole-Ph-Fc), 8.36 (d, *J* = 8.0 Hz, 2H, *m*-Ph), 8.22 (d, *J* = 8.0 Hz, 2H, *o*-Ph), 5.37 (s, 2H, α-Cp₂), 5.34 (s, 4H, α-Cp_{1,3}), 4.82 (s, 2H, β-Cp₂), 4.79 (s, 4H, β-Cp_{1,3}), 4.13 (s, 5H, CpH₂), 4.11 (s, 10H, CpH_{1,3}). ¹³C NMR (101 MHz, DMSO-d₆, δ): 167.75 (C-carboxylic acid), 149.70 (α-pyrrole-Ph-Fc), 149.23 (α-pyrrole-Fc-Fc), 148.94 (α-pyrrole-Fc-Fc), 147.46 (*i*-Ph), 147.33 (α-pyrrole-Ph-Fc), 134.20 (*o*-Ph), 132.11 (β-pyrrole-Ph-Fc), 131.30 (β-pyrrole-Fc-Fc), 131.22 (β-pyrrole-Fc-Fc), 129.82 (β-pyrrole-Ph-Fc), 127.65 (*m*-Ph), 118.79 (meso-C-Ph), 118.04 (meso-C-Fc₂), 117.53 (meso-C-Fc_{1,3}), 90.50 (C_i-Cp₂), 90.21 (C_i-Cp_{1,3}), 77.19 (α-Cp₂), 76.97 (α-Cp_{1,3}), 70.35 (CpH), 68.58 (β-Cp_{1,3}), 68.52 (β-Cp₂). MS (MALDI-TOF, DCTB matrix, *m/z*): [M]⁺ 1044.0, [M+O+H]⁺ 1061.0. HREI+ (*m/z*): [M]⁺ 1044.0495, calcd for C₅₇H₄₀Fe₃N₄O₂Zn: 1044.0486. Elemental analysis calcd for C₅₇H₄₀Fe₃N₄O₂Zn: C 65.46, H 3.85, N 5.36, found: C 66.54, H 4.21, N 5.19. Atomic absorption calcd for C₅₇H₄₀Fe₃N₄O₂Zn: Fe 16.0, found: Fe 15.5. FTIR (cm⁻¹) 622 (m), 646 (w), 720 (s), 767 (sh), 794 (vs), 810 (sh), 821 (sh), 874(w), 923 (m), 999 (s), 1030 (w), 1058 (m), 1079 (w), 1107 (m), 1176 (sh), 1191 (w), 1216 (w), 1236 (w), 1264 (w), 1291 (sh), 1312 (w), 1337 (w), 1353 (w), 1389 (w), 1410 (w), 1484 (m), 1565 (w), 1605 (m), 1689 (s), 1730 (sh), 2929 (vw), 3090 (br).

Acknowledgements

We thank Newcastle University and Nottingham University for financial support, FP7-PEOPLE-2009-IRSES grant (246902) and Academy of Finland grant (263486) for funding to cover the exchange of researchers. The EPSRC UK National Mass Spectrometry Facility at Swansea University is thanked for collecting mass spectra of compounds.

Notes and references

- ^a Institute of Chemistry, Academy of Sciences of Moldova, 3, Academiei str., Chisinau, Republic of Moldova, MD-2028
- ^b Molecular Photonics Laboratory, School of Chemistry, Newcastle University, Newcastle-upon-Tyne, NE1 7RU, UK,
- ^c Department of Chemistry and Engineering, Tampere University, Tampere, Finland.
- ^d School of Chemistry, The University of Nottingham, Nottingham, NG7 2RD, UK.

Electronic Supplementary Information (ESI) available: [Additional molecular orbital calculations, cyclic voltammogram and time-resolved spectra]. See DOI: 10.1039/b000000x/

- 1 M. R. Wasielewski. *Chem. Rev.*, 1992, **92**, 435; J. E. Mullet, J. J. Burke and C. J. Arntzen, *Plant Physiol.* 1980, **65**, 814.

- 2 A. Kay and M. Grätzel. *J. Phys. Chem.*, 1993, **97**, 6272; A. Tsuda and A. Osuka. *Science*, 2001, **293**, 79; W. M. Campbell, A. K. Burrell, D. L. Officer and K. W. Jolley. *Coord. Chem. Rev.*, 2004, **248**, 1363; C.-P. Hsieh, H.-P. Lu, C.-L. Chiu, C.-W. Lee, S.-H. Chuang, C.-L. Mai, W.-N. Yen, S.-J. Hsu, E. Wei-Guang Diao and C.-Y. Yeh, *J. Mater. Chem.* 2010, **20**, 1127; K. Kadish, K. Smith, R. Guillard, (eds). *The Porphyrin Handbook*. Academic Press, 2000, volume 6.
- 3 D. Gust, T. A. Moore, A. L. Moore. *Acc. Chem. Res.*, 2001, **34**, 40; J. H. Alstrum-Acevedo, M. K. Brennaman and T. J. Meyer, *Inorg. Chem.*, 2005, **44**, 6802; H. Imahori, T. Umeyama and S. Ito. *Acc. Chem. Res.*, 2009, **42**, 11.
- 4 M. E. El-Khouly, O. Ito, P. M. Smith and F. D'Souza, *J. Photochem. Photobiol. C: Photochem. Rev.*, 2004, **5**, 79; D. M. Guldi, *Chem. Soc. Rev.*, 2002, **31**, 22.
- 5 P. K. Poddutoori, A. S. D. Sandanayaka, T. Hasobe, O. Ito and A. van der Est, *J. Phys. Chem. B*, 2010, **114**, 14348; M. U. Winters, E. Dahlstedt, H. E. Blades, C. J. Wilson, M. J. Frampton, H. L. Anderson and B. Albinsson, *J. Am. Chem. Soc.*, 2007, **129**, 4291.
- 6 H. Imahori, *Org. Biomol. Chem.*, 2004, **2**, 1425; J. Springer, G. Kodis, L. de la Garza, A. L. Moore, T. A. Moore and D. Gust, *J. Phys. Chem. A*, 2003, **107**, 3567.
- 7 Y. Kubo, M. Yamamoto, M. Ikeda, M. Takeuchi, S. Shinkai, S. Yamaguchi and K. Tamao, *Angew. Chem. Int. Ed.*, 2003, **42**, 2036; A. Mills and A. Lepre, *Anal. Chem.*, 1997, **69**, 4653; R. Prasad, V. K. Gupta and A. Kumar, *Anal. Chim. Acta.*, 2004, **508**, 61.
- 8 R. R. Allison, G. H. Downie, R. Cuenca, X.-H. Hu, C. J. H. Childs and C. H. Sibata, *Photodiagnosis and Photodynamic Therapy*, 2004, **1**, 27; E. S. Nyman and P. H. Hynninen, *J. Photochem. Photobiol. B: Biology*, 2004, **73**, 1.
- 9 L. Giribabu and R. K. Kanaparthi, *Current Science*, 2013, **7**, 847; S.-L. Wu, H.-P. Lu, H.-T. Yu, S.-H. Chuang, C.-L. Chiu, C.-W. Lee, E. Wei-Guang Diao and C.-Y. Yeh, *Energy Environ. Sci.*, 2010, **3**, 949; C.-W. Lee, H.-Pei Lu, C.-M. Lan, Y.-L. Huang, Y.-R. Liang, W.-N. Yen, Y.-C. Liu, Y.-S. Lin, E. Wei-Guang Diao and C.-Y. Yeh, *Chem. Eur. J.* 2009, **15**, 1403; L.-L. Li and E. Wei-Guang Diao, *Chem. Soc. Rev.*, 2013, **42**, 291; A. Yella, H.-W. Lee, H. N. Tsao, C. Yi, A. K. Chandiran, K. Nazeeruddin, E. Wei-Guang Diao, C.-Y. Yeh, S. M. Zakeeruddin and M. Grätzel, *Science*, 2011, **334**, 629.
- 10 J. A. Baxter, *J. Vac. Sci. Techn. A*, 2012, **30**, 020801.
- 11 S. E. Koops, B. C. O'Regan, P. R. F. Barnes and J. R. Durrant, *J. Am. Chem. Soc.*, 2009, **131**, 4808.
- 12 M. Wang, P. Chen, R. Humphry-Baker, S. M. Zakeeruddin and M. Grätzel, *ChemPhysChem*, 2009, **10**, 290.
- 13 S. A. Haque, E. Palomares, B. M. Cho, A. N. M. Green, N. Hirata, D. R. Klug and J. R. Durrant, *J. Am. Chem. Soc.*, 2005, **127**, 3456; M. Grätzel, *J. Photochem. Photobiol. A: Chemistry*, 2004, **164**, 3; M. Grätzel, *J. Photochem. Photobiol. C: Photochem. Rev.* 2003, **4**, 145; A. Sarto Polo, M. K. Itokazu and N. Y. M. Iha, *Coord. Chem. Rev.*, 2004, **248**, 1343.
- 14 H. Tian, X. Yang, J. Pan, R. Chen, M. Liu, Q. Zhang, A. Hagfeldt and L. Sun, *Adv. Funct. Mater.*, 2008, **18**, 3461.
- 15 R. van Grondelle, J. P. Dekker, T. Gillbro and V. Sundstrom, *Biochim. Biophys. Acta.*, 1994, **1187**, 1.
- 16 R. Argazzi, N. Y. M. Iha, H. Zabri, F. Odobel and C. A. Bignozzi. *Coord. Chem. Rev.*, 2004, **248**, 1299.
- 17 V. A. Nadtochenko, D. V. Khudyakov, N. V. Abramova, E. V. Vorontsov, N. M. Loim, F. E. Gostev, D. G. Tovbin, A. A. Titov and O. M. Sarkisov, *Russ. Chem. Bull. Int. Ed.*, 2002, **6**, 986.
- 18 K. Kadish, K. Smith and R. Guillard, R. (eds). *The Porphyrin Handbook*. Academic Press, 2000, volume 1.
- 19 G. R. Geier III, B. J. Littler and J. S. Lindsey, *J. Chem. Soc., Perkin Trans. 2*, 2001, Part 1-4, 677.
- 20 S. J. Narayanan, S. Venkatraman, S. R. Dey, B. Sridevi, V. R. G. Anand and T. K. Chandrashekar, *Synlett*, 2000, **12**, 1834.
- 21 V. N. Nemykin, G. T. Rohde, C. D. Barrett, R. G. Hadt, J. R. Sabin, G. Reina, P. Galloni and B. Floris, *Inorg. Chem.* 2010, **49**, 7497.
- 22 R. Slota, M. A. Broda, G. Dyrda, K. Ejsmont and G. Mele, *Molecules*, 2011, **16**, 9957.
- 23 V. N. Nemykin and R. G. Hadt. *J. Phys. Chem. A.*, 2010, **114**, 12062.
- 24 F. Rocquet, L. Berreby and J. P. Marsault, *Spectrochim. Acta*, 1973, **29A**, 1101; A. Haaland and J.-E. Nilsson, *J. Chem. Soc., Chem. Commun. (London)*, 1968, 88.
- 25 M. Gouterman and G. H. Wagnière, *J. Mol. Spectros.* 1963, **11**, 108.
- 26 V. N. Nemykin, G. T. Rohde, C. D. Barrett, R. G. Hadt, C. Bizzarri, P. Galloni, B. Floris, I. Nowik, R. H. Herber, A. G. Marrani, R. Zanoni and N. M. Loim, *J. Am. Chem. Soc.* 2009, **131**, 14969; G. T. Rohde, J. R. Sabin, C. D. Barrett and V. N. Nemykin, *New J. Chem.*, 2011, **35**, 1440.
- 27 M. Nappa and J. S. Valentine, *J. Am. Chem. Soc.*, 1978, **100**, 5075.
- 28 V. N. Nemykin, P. Galloni, B. Floris, C. D. Barrett, R. G. Hadt, R. Subbotin, A. G. Marrani, R. Zanoni and N. M. Loim, *Dalton Trans.*, 2008, 4233.
- 29 V. I. Goldanskii and R. H. Herber. *Химические применения мессбауэровской спектроскопии*. Издат. "МИР". Translation from English by V.I. Goldanskii, 1970, 232.
- 30 P. Neta, A. Scherz and H. Levanon, *J. Am. Chem. Soc.*, 1979, **101**, 3624; G. L. Closs and L. E. Closs, *J. Am. Chem. Soc.*, 1963, **85**, 818.
- 31 K. Kiyosawa, N. Shiraishi, T. Shimada, D. Masui, H. Tachibana, S. Takagi, O. Ishitani, D. A. Tryk and H. Inoue, *J. Phys. Chem. C* 2009, **113**, 11667; M. Kubo, Y. Mori, M. Otani, M. Murakami, Y. Ishibashi, M. Yasuda, K. Hosomizu, H. Miyasaka, H. Imahori and S. Nakashima, *J. Phys. Chem. A*, 2007, **111**, 5136; A. Harriman, M. Hissler, O. Trompette and R. Ziessel, *J. Am. Chem. Soc.*, 1999, **121**, 2516; A. C. Benniston, A. Harriman and P. Li, *J. Am. Chem. Soc.*, 2010, **132**, 26.

- 32 A. S. Hart, B. Chandra, K. C Habtom, B. Gobeze, L. R. Sequeira and F. D'Souza, *Appl. Mater. Interfaces*, 2013, **5**, 5314.
- 33 The strong electronic coupling is also in fitting with the strong ground state charge transfer character which results in the CT absorption band.
- 34 E. A. Gibson, A. L. Smeigh, L. Le Pleux, L. Hammarström, F. Odobel, G. Boschloo and A. Hagfeldt, *J. Phys. Chem. C.*, 2011, **115**, 9772.
- 35 S. M. Feldt, P. W. Lohse, F. Kessler, M. K. Nazeeruddin, M. Grätzel, G. Boschloo and A. Hagfeldt, *Phys. Chem. Chem. Phys.*, 2013, **15**, 7087.
- 36 J. P. Harney, T. Dransfield and J. Rochford, *Tetrahedron Lett.*, 2013, **53**, 4700.
- 37 Gaussian 03, M. J. Frisch, G. W. Trucks, H. B. Schlegel, G. E. Scuseria, M. A. Robb, J. R. Cheeseman, J. A. Montgomery, Jr., T. Vreven, K. N. Kudin, J. C. Burant, J. M. Millam, S. S. Iyengar, J. Tomasi, V. Barone, B. Mennucci, M. Cossi, G. Scalmani, N. Rega, G. A. Petersson, H. Nakatsuji, M. Hada, M. Ehara, K. Toyota, R. Fukuda, J. Hasegawa, M. Ishida, T. Nakajima, Y. Honda, O. Kitao, H. Nakai, M. Klene, X. Li, J. E. Knox, H. P. Hratchian, J. B. Cross, V. Bakken, C. Adamo, J. Jaramillo, R. Gomperts, R. E. Stratmann, O. Yazyev, A. J. Austin, R. Cammi, C. Pomelli, J. W. Ochterski, P. Y. Ayala, K. Morokuma, G. A. Voth, P. Salvador, J. J. Dannenberg, V. G. Zakrzewski, S. Dapprich, A. D. Daniels, M. C. Strain, O. Farkas, D. K. Malick, A. D. Rabuck, K. Raghavachari, J. B. Foresman, J. V. Ortiz, Q. Cui, A. G. Baboul, S. Clifford, J. Cioslowski, B. B. Stefanov, G. Liu, A. Liashenko, P. Piskorz, I. Komaromi, R. L. Martin, D. J. Fox, T. Keith, M. A. Al-Laham, C. Y. Peng, A. Nanayakkara, M. Challacombe, P. M. W. Gill, B. Johnson, W. Chen, M. W. Wong, C. Gonzalez, and J. A. Pople, Gaussian, Inc., Wallingford CT, 2004.

Graphical Abstract

